© Universiti Tun Hussein Onn Malaysia Publisher's Office

IJIE

http://penerbit.uthm.edu.my/ojs/index.php/ijie
ISSN : 2229-838X e-ISSN : 2600-7916

The International Journal of Integrated Engineering

Simplified Model Predictive Current Control for Surface-Mounted Permanent-Magnet Synchronous Motor Drives with Adaptive Duty Modulation

Crestian Almazan Agustin[1*]

[1]Department of Electrical Engineering,
Isabela State University, City of Ilagan, Isabela, 3300 PHILIPPINES

*Corresponding Author

DOI: https://doi.org/10.30880/ijie.2023.15.04.019
Received 29 June 2022; Accepted 3 August 2023; Available online 28 August 2023

Abstract: Parameter control and cost minimization are among the significant aspects of model predictive current controllers. However, with the conventional control scheme involving a fixed switching vector application, susceptibility to uncontrolled and fluctuating current ripples remains a primary concern. This paper presents a simplified approach of the model predictive current controller based on adaptive duty modulation for the surface-mounted permanent-magnet synchronous motor (SPMSM). In this method, the implementation of two successive synthesized voltage vectors in each control period adopts the adaptive soft-switching combination relative to calculated optimal duty ratios. Experimental results validate performance improvement and optimize current prediction accuracy.

Keywords: Surface-mounted permanent-magnet synchronous motor, model predictive current controller, adaptive voltage vector application, microcontroller

1. Introduction

Over the last decades, surface-mounted permanent-magnet synchronous motors (SPMSM) have been observed as superior solutions to highly demanding extensive drive applications. Due to their advantageous characteristics of high efficiency, excellent power density, robustness, and low noise, SPMSM has become auspicious in various industrial applications such as manufacturing, renewable energy, and electric vehicles, among others [1]-[2].

Several control strategies have been developed for SPMSM to maximize its functionality and dynamic performance. Compared with other control strategies, the issue of non-linear components and other fundamental constraints cannotbe disregarded in the control system structure. Direct torque control and field-oriented control, popularly known as the DTC and FOC, are widely employed. However, these two are linear controllers and are not reliable for highly non- linear systems of electric motor drive systems [3]-[5]. Meanwhile, an emerging control method is gaining broader attention in the field of power converters due to its constraint-free and straightforward implementation, and that is the model predictive current controller (MPCC). The MPCC is getting a bigger audience in various research undertakings due to the fact that most motor drive systems are adopting power converters for operations [6]. Similarly, the onset of semiconductor-based power conversion devices has helped optimize the quality, performance, and stability of several industrial applications. These power converters are of different types and sizes depending on the conversion mechanisms relative to the alternating current and the direct current relationships. As a result, most emerging technologies have digitally replaced analog control systems with power transistors capable of ultra-fast switching frequencies [7]-[10].

While power converters remain an enabling technology, their control operation mainly depends on the quality of the projected inner current loop, making it highly compatible with MPCC. The MPCC offers advantageous features of

*Corresponding author: 20753004@email.ntou.edu.tw

excellent dynamic response and simple optimization criteria. The implementation of the controller is based on its system models and parameters to forecast the future behaviors of the controlled variables according to the predefined prediction time horizon. This can be implemented by the discrete representation of parameters to select the optimal response relative to the least possible cost function value.

The control scheme of MPCC is widely known for its simplicity, high dynamic performance, and effective cost-function minimization [11]-[12]. The performance of parameter control can achieve significant improvement and optimization; however, in [9], the standard selection mode of the active or applied voltage vector is restricted from predefined values by the voltage source inverter. Similar to [10], a variable and finite-state output using a single input voltage vector in every sampling period can directly affect the dynamic response and robust control of the system. A modulation-based MPCC is proposed in [13], in which two successive voltage vectors are applied every sampling period, boosting the candidate switching modes up to thirteen compared to the conventional scheme of only seven. The application of multiple voltage vectors within the control period is observed to yield a significant improvement in both steady-state and dynamic (transient state) performances, but the predictive scheme presented applies the fixed and switching duration. Other modulation methods are presented in [14] and [15] that integrate duty calculation to reduce prediction error. Parvathy, et al. [14], designed a modified duty-based MPCC by employing combined switching action of active and null voltage vectors. In [15], the MRAS or the model reference adaptive system is alternatively worked as a voltage control instrument and flux weakening control of the motor drive. However, these proposed methods [14]-[15] increase candidate voltage vectors and use complicated control algorithms that result in heavier calculation complexity in its voltage vector optimization.

The current predictive controllers attain an impressive tracking capability under the steady-state condition of stator current. Thanks to the onset of powerful and high-speed operating frequencies of current digital signal processors nowadays, limitations from heavy computational loadings can be overcome, making the predictive current control strategy advance in theory and application. One of which is the model-free prediction current controller [16]. This method of stator current prediction utilizes the stored current difference obtained from the switching commands of inverter signals using current sensors. The current tracking performance is improved in [17], where prediction error correction guarantees an optimal voltage vector selection based on time delay compensation. However, similar to other control methods, the challenge of meeting the minimum requirement of the low current ripple is at stake due to limited and fixed switching durations. Hence, to achieve a flexible switching application of each applied voltage vector, an adaptive voltage vector application is proposed in this paper, known as the model predictive current control based on adaptive duty modulation (ADM-MPCC).

In this work, the adaptive control of the model-based approach can be realized from the duty cycle duration of applied voltage vectors using a modulated and variable switching duration in each control sampling period. In this way, the proposed method implements the selection of seven voltage vectors that are modulated in two successive durations corresponding to their optimal duty cycle.

2. Methodological Formulation of Adaptive Duty Modulation

The equivalent structure and circuit diagram of a six-switch three-phase inverter-fed SPMSM in the *a-b-c* reference frame is illustrated in Fig. 1. The three-phase components and variables are described accordingly as follows: v_{as}, v_{bs}, v_{cs} are the stator voltages, r_s is the stator resistance, $L_{aa,} L_{bb}, L_{cc}$ are the mutual inductances, θ_{re} denotes the rotor angle, ω_{re} represent the angular speed, and v_{DC} for the dc-link voltage.

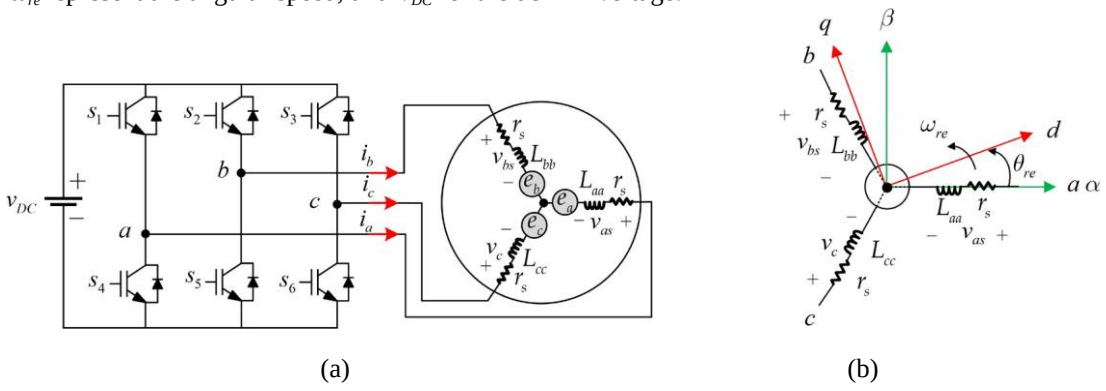

(a) (b)

Fig. 1 - The six-switch three-phase (SSTP) inverter-fed SPMSM. (a) The equivalent circuit diagram, and (b) reference frames of stator circuit in α-β and *d-q*

The three-phase stator voltage equation based on a mathematical model can independently be written as [3],

$$v_{as} = r_s i_{as} + \frac{d\lambda_{as}}{dt} \tag{1}$$

$$v_{bs} = r_s i_{bs} + \frac{d\lambda_{bs}}{dt} \tag{2}$$

$$v_{cs} = r_s i_{cs} + \frac{d\lambda_{cs}}{dt} \tag{3}$$

where i_{as}, i_{bs}, i_{cs} denotes the stator currents, and $\lambda_{as}, \lambda_{bs}, \lambda_{cs}$ are the stator fluxes dependent on the effect of mutual inductance. For simple representation, the voltage vectors are converted into their equivalent $\alpha - \beta$ and expressed as reference frame

$$v_x = r_s i_x + L_q \frac{d}{dt} i_x + e_x, x \in \{\alpha, \beta\} \tag{4}$$

where L_q and e_x are the *q*-axis inductance and the back-EMF, respectively. Following the above formulation, (4) can be
explicitly reconstructed in its time-discrete equivalent form in [*k*]th horizon. The discretized stator voltage is deducedaccordingly as

$$v_{\alpha s}[k] = r_s i_{\alpha s}[k] + L_s \frac{i_{\alpha s}[k] - i_{\alpha s}[k-1]}{T_s} + e_\alpha[k] \tag{5}$$

$$v_{\beta s}[k] = r_s i_{\beta s}[k] + L_s \frac{i_{\beta s}[k] - i_{\beta s}[k-1]}{T_s} + e_\beta[k] \tag{6}$$

According to (5) and (6), the discretized equation of the stator voltages varied based on applied switching states, as shown in Fig. 2. The vector representation comprises six unique active voltage vectors and two zero vectors described in Table 1. Theoretically, two zero vectors are available from the actuation of power switches in the inverter but of similar characteristics. Hence, vectors v_0 and v_7 are treated equally.

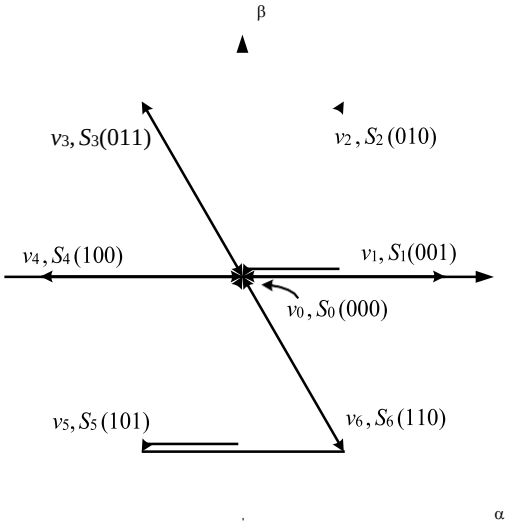

Fig. 2 - Switching distribution of basic voltage vectors of the six-switch three-phase voltage source inverter

Table 1 - Switching states of basic voltage vectors

Voltage Vectors	Switching States		Equivalent Voltages	
v_x	S_x	$S_aS_bS_c$	v_α	v_β
v_0	S_0	000	0	0
v_1	S_1	001	$V_{DC}/3$	$-\sqrt{3}V_{DC}/3$
v_2	S_2	010	$V_{DC}/3$	$\sqrt{3}V_{DC}/3$
v_3	S_3	011	$2V_{DC}/3$	0
v_4	S_4	100	$-2V_{DC}/3$	0
v_5	S_5	101	$-V_{DC}/3$	$-\sqrt{3}V_{DC}/3$
v_6	S_6	110	$-V_{DC}/3$	$\sqrt{3}V_{DC}/3$
v_7	S_7	111	0	0

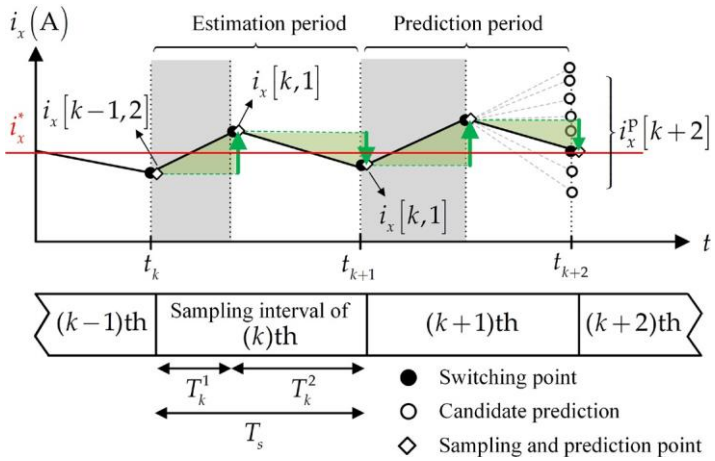

Fig. 3 - Schematic diagram of vector application in an adaptive duty modulation

As illustrated in Fig. 3, the adaptive duty modulation is implemented from the application of two applied voltage vectors in each control period with adjustable conduction duration. Similarly, to compensate for the time delay, the current sampling and measurement are performed after activation of the inverter to avoid the current surge caused by inverter switching [11]. This scheme permits two identical or different active voltage vectors at a given [k]th sampling period, T_S . Their switching durations can be controlled in a variable and flexible depending on the calculated optimal time, T_k^1 and T_k^2, which corresponds respectively to the conduction time of the two applied voltage vectors. The superscript "1" and "2" denotes the sequence of the first and second applications. The mathematical relation ofswitching time can be described as

$$T^1 + T^2 = \tag{7}$$

In terms of duty ratios, these can be expressed as D^1 and D^2. The duty ratios can be obtained relative to (7) and the

total sampling period. The expression is given as,

$$\begin{aligned} D_k^1 &= T_k^1 / T_s \\ D_k^2 &= T_k^2 / T_s \end{aligned} \tag{8}$$

From (8), it is obvious that the permitted range of duty ratios of D_k^1 and D_k^2 is between 0 and 1, that is, $D_k^1, D_k^2 \in [0,1]$. Applying the duty ratios obtained from (8), the resulting synthesized voltage vector can be discretely depicted as,

$$v^c[k] = D^1 v\ [k,1] + D^2 v\ [k,2] \tag{9}$$

where $v_x[k,1]$ and $v_x[k,2]$, $x \in \{\alpha, \beta\}$ are the stator voltages corresponding to the first and second applied voltage vectors in [k]th period, respectively. The superscript "c" in (9) denotes the synthesized voltage vector comprising two applied basic voltage vectors of the inverter, described in Table 1. Based on (7) and (8), the same expression can be
validly defined in the $[k+1]$th sampling period as,

$$D^1_{k+1} + D^2_{k+1} = 1 \tag{10}$$

Similarly, duty ratios described in (11) can be used to estimate the voltage vector prediction in $[k+1]$th as,

$$v^c_x[k+1] = D^1_{k+1} v_x[k+1,1] + D^2_{k+1} v_x[k+1,2] \tag{11}$$

By applying the compensated time delay, the definition of (5) and (6) can be reformulated to predict the stator current value in the $[k+2]$th sampling period

$$i^p_x[k+2] = \frac{1}{\left(r_s T_s + L_q\right)}\left(L_q i^p_x[k+1] + T_s v^c_x[k+1] - T_s \hat{e}_x[k]\right) \tag{12}$$

Finally, the resulting optimization criterion of cost function G can be derived as

$$G = \left(i^*_\alpha[k] - i^p_\alpha[k+2]\right)^2 + \left(i^*_\beta[k] - i^p_\beta[k+2]\right)^2 \tag{13}$$

In this paper, the reference frame of *α-β* stator current is used to calculate and select optimal switching combinations with minimal cost value. The optimal combination of voltage vectors is interpreted *via* switching reactions of the inverter and used for the next sampling period. Moreover, the simplified control diagram of the ADM-MPCC method isdescribed in Fig. 4. The selection of *α-β* from the three-phase stationary *a-b-c* reference frame is to make calculations straightforward and direct. This strategy allows the independent control of motor parameters, such as voltage, current, and flux, and assumes coupling effects negligible [3]. The two-phase *α-β* retains its sinusoidal characteristics and phase shifted 90 degrees apart in a stationary frame, making it straightforward in modeling the motor relative to the six-switch three-phase inverter. As a result, voltage characteristics of the SPMSM are obtained based on the switching combinations of the six-switched inverter, called voltage vector is described in Fig. 2.

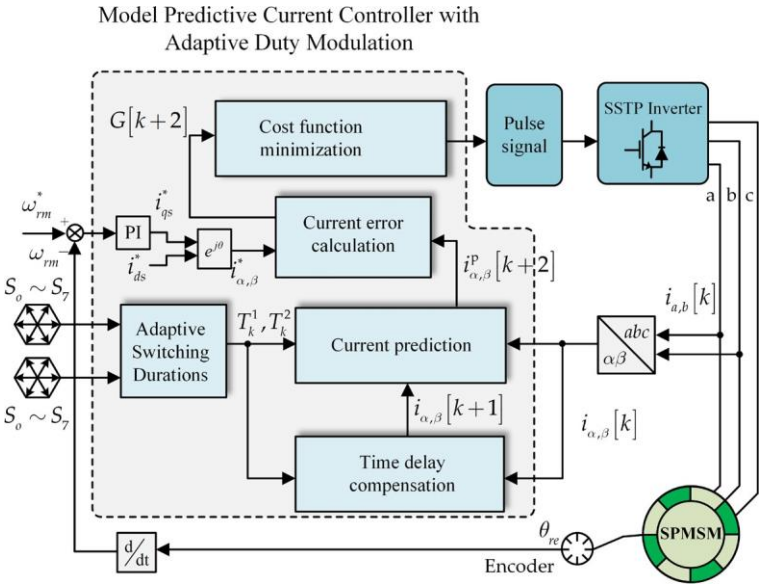

Fig. 4 - Simplified block diagram of model predictive current controller based on adaptive duty modulation (ADM- MPCC)

3. Experimental Validations and Performance Metrics

Control performance and assessment of the proposed ADM-MPCC are conducted using the experimental test bench shown in Fig. 5. It comprises three main parts: the SPMSM as the load motor, the motor drive circuit, and the power meter and load-torque control unit. In particular, the TMS320F28379D digital signal processor is carried out along with the prototype drive system composed of the following subcomponents: (A) SPMSM coupled with adjustable load- torque switch; (B) Computer or working unit; (c) Load-torque controller for automatic load application; (D) Motor drive circuit board; (E) Oscilloscope, and (F) Programmable DC power supply. The sampling interval set for the microcontroller is 100 µs and 200V for the dc link voltage. The fundamental specification of the SPMSM is shown in detail in Table 2.

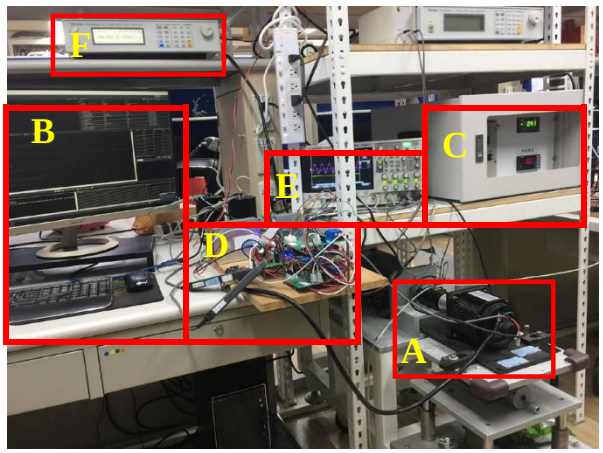

Fig. 5 - Experimental set-up

Table 2 - SPMSM specification

Parameters	Symbol	Value
Rated power	HP	0.5
Rated frequency	Hz	60
Pole Number	pole	4
Rated torque	Nm	1.176
Rated speed	rpm	1800
d-axis inductance	*m*H	24.76
q-axis inductance	*m*H	45.33
Stator resistance	Ω	6.8

The assessment and comparison of the performance of the proposed ADM-MPCC relative to other predictive controllers are performed based on the three performance metrics employed, namely the average current ripple (ACR), the average current error (ACE), and the current total harmonic distortion (THD*i*). The ACR measures the root-mean-square or the effective measurement of the current error. ACE is used to quantify the tracking performance of the predictive controllers corresponding to the current command value or reference ($i_x^*, x \in \{\alpha,\beta\}$), and the THDi, commonly expressed in percentage (%), measures the harmonic distortion concerning the fundamental frequency. Analytically, these metrics are defined as follows:

For the average current ripple (ACR):

$$ACR_{i_\alpha} = \sqrt{\frac{1}{N}\sum_{k=1}^{N}\left(i_\alpha^{ref}(k) - i_\alpha(k)\right)^2} \tag{14}$$

$$ACR_{i_\beta} = \sqrt{\frac{1}{N}\sum_{k=1}^{N}\left(i_\beta^{ref}(k) - i_\beta(k)\right)^2} \quad (15)$$

$$ACR_{i_{\alpha\beta}} = \frac{1}{2}\left(ACR_{i_\alpha} + ACR_{i_\beta}\right) \quad (16)$$

For the average current error (ACE):

$$ACE_{i_\alpha} = \frac{1}{N}\sum_{k=1}^{N}\left|i_\alpha^{ref}(k) - i_\alpha(k)\right| \quad (17)$$

$$ACE_{i_\beta} = \frac{1}{N}\sum_{k=1}^{N}\left|i_\beta^{ref}(k) - i_\beta(k)\right| \quad (18)$$

$$ACE_{i_{\alpha,\beta}} = \frac{1}{2}\left(ACE_{i_\alpha} + ACE_{i_\beta}\right) \quad (19)$$

For the current total harmonic distortion (THD*i*):

$$THDi(\%) = \frac{1}{2}\left[\frac{\sqrt{\sum_{h=2}^{30} I_{\alpha h}^2}}{I_{\alpha 1}} + \frac{\sqrt{\sum_{h=2}^{30} I_{\beta h}^2}}{I_{\beta 1}}\right] \times 100\% \quad (20)$$

where N represents the total sampling points, h for the harmonic order, $I_{\alpha 1}$ and $I_{\beta 1}$ is the current measurement in thefirst harmonic order in α-β.

4. Results and Discussions

Experimental validation and discussion are presented herein based on the performance of the ADM-MPCC relative tothe conventional or classical predictive scheme of MPCC. Stator current behaviors under steady-state and transient responses are investigated and analyzed while tracking the reference value. The steady-state tests include the following: current command of 4A at 30Hz in Fig. 6 and current command of 4A at 10Hz in Fig. 7. The transient response includes the current command at 10Hz with the α-axis current reversal from -4A to 4A at 0.05s in Fig. 8 and the current command at 10 Hz with amplitude jumping from 1A to 4A at 0.2s in Fig. 9. Moreover, additional experiments are shown under the speed commands of low-speed of 200rpm and high speed of 1200rpm, both operating at a load-torque of 1.0Nm.

The experimental waveforms of the current responses on both control schemes of MPCC and proposed ADM-MPCC are shown in Fig. 6-9. The two methods are designed to track the α-β current reference value under various test commands at a stable load and step response. The performance indices used to evaluate performances are the ACR, ACE, and %THD*i*. Fig. 6-7 illustrates the current response in steady-state at different operating frequencies of 30Hz and 10Hz. Results showed that the proposed method of ADM-MPCC yields a better predictive response with improved ripple reduction, better error accuracy, and lesser THD*i*. In particular, the ACR, ACE, and %THD*i* in Fig. 6, have recorded an improvement from the conventional MPCC by 41.49%, 30.60%, and 39.74%, respectively. Similarly, at a lower speed with a sampling frequency of 10Hz, the current ripples are evidently refined using the proposed method, yielding a 40.16% reduction. As a result, the current error, which is one of the important indicators in the predictive controller, has been greatly reduced and recorded current harmonics are also lower.

Further comparisons have been made under the current command *via* analysis of the transient response. Fig. 8 describes the implementation of the current reversal command in the α-axis from -4A to 4A, while Fig. 9 operates the current step from 1A and 4A. Accordingly, the proposed method outperformed the conventional ones, with impressive current ripple reductions, minimized current errors, and lower harmonic distortions. From the quantitative results, Table 3 shows the performance between the traditional MPCC and the proposed ADM-MPCC.

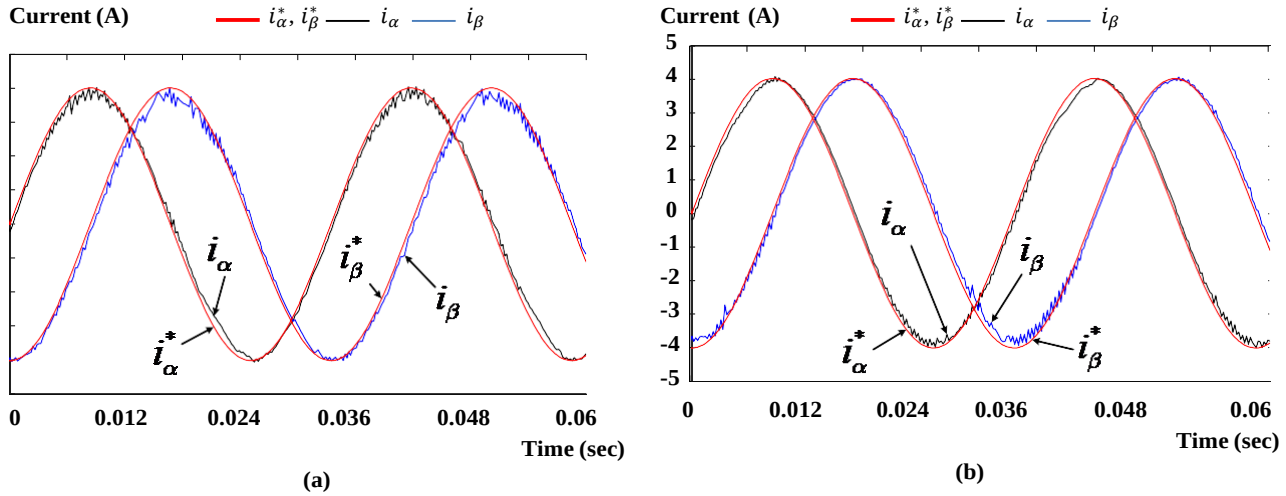

Fig. 6 - Experimental waveforms under the current command of 4A and operating frequency of 30 Hz (a) MPCC; (b) ADM-MPCC

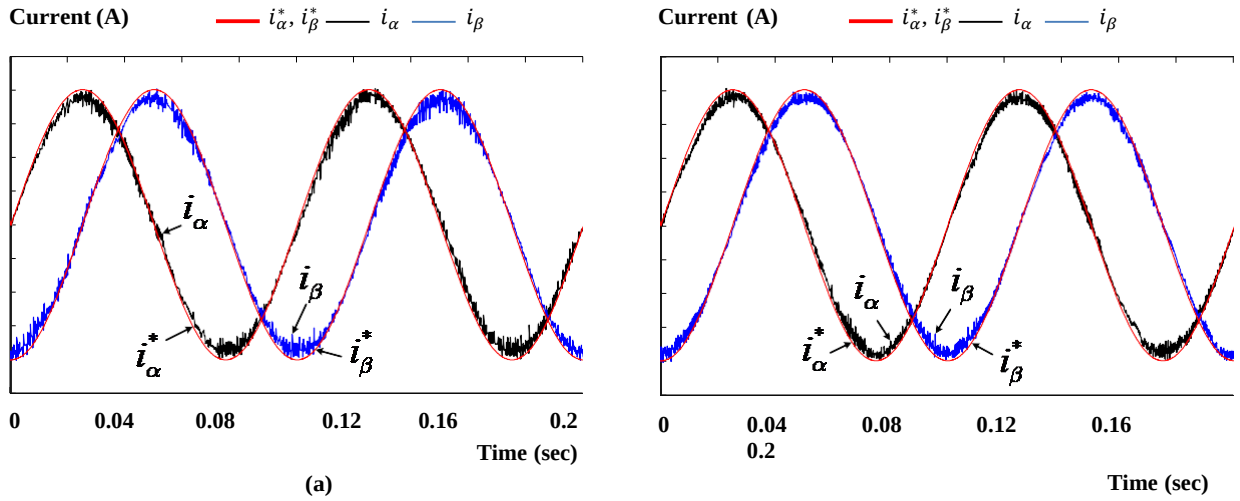

Fig. 7 - Experimental waveforms under the current command of 4A and operating frequency of 10 Hz (a) MPCC; (b) ADM-MPCC

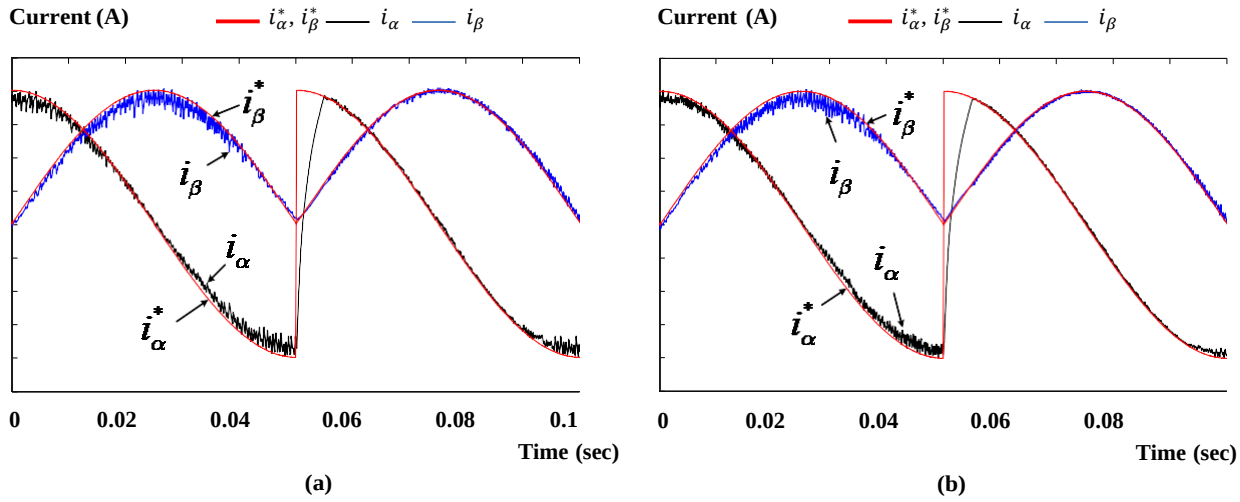

Fig. 8 - Experimental waveforms under the current reversal command in α-axis from -4A to 4A at 0.05 seconds (a)MPCC; (b) ADM-MPCC

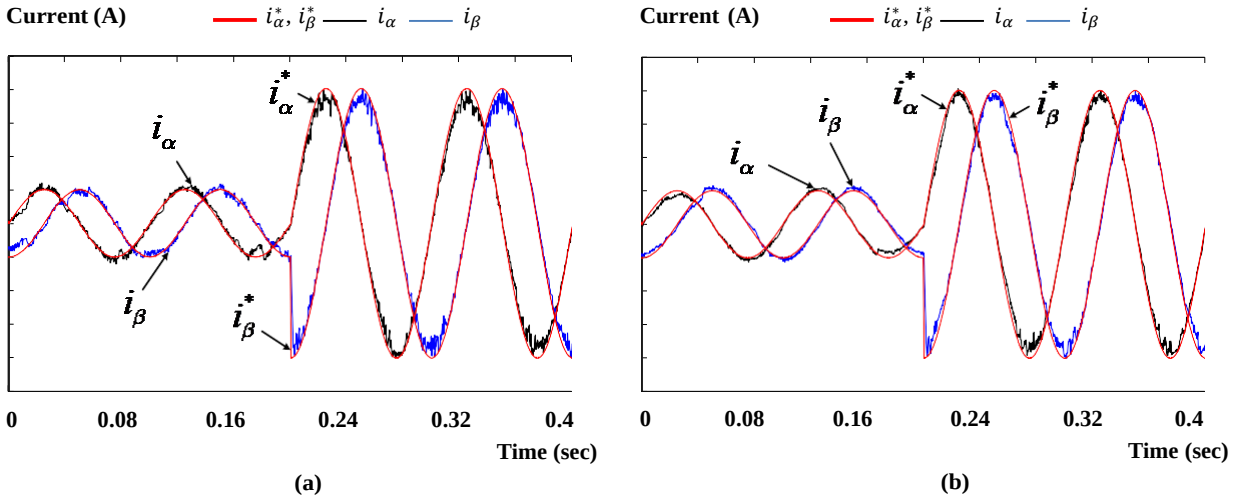

Fig. 9 - Experimental waveforms under the current step command from 1A to 4A at 0.2 seconds (a) MPCC; (b) ADM-MPCC

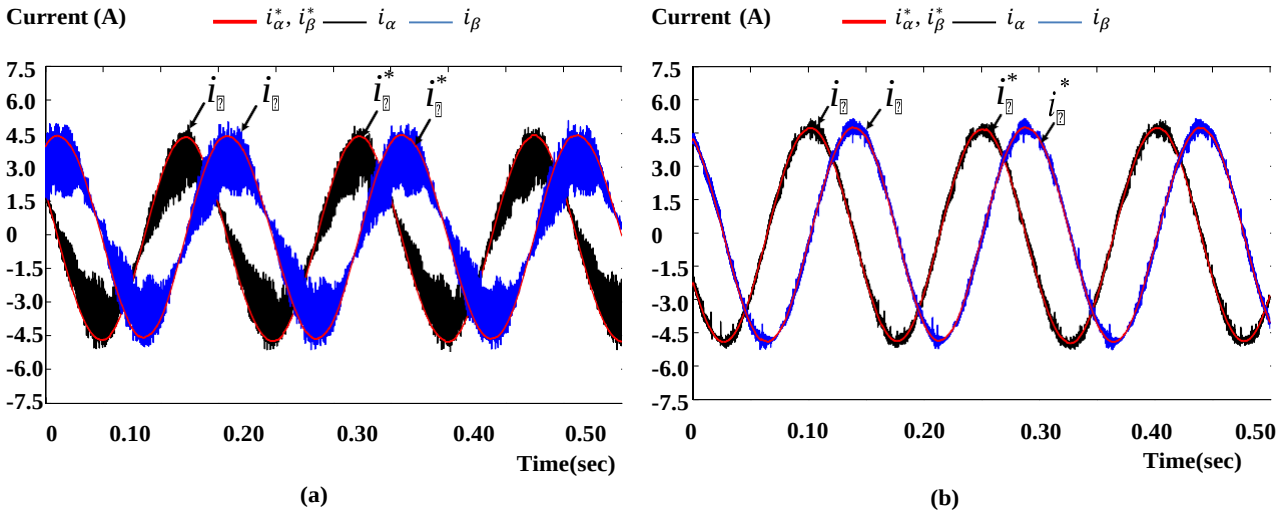

Fig. 10 - Experimental waveforms under low-speed command of 200 rpm and load-torque of 1.0 N (a) MPCC; (b) ADM-MPCC

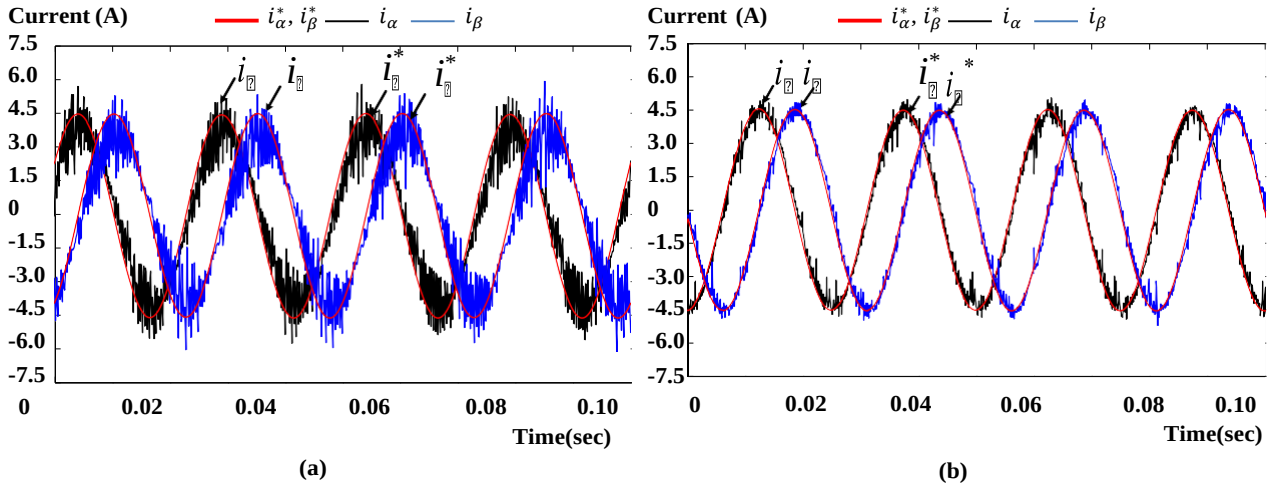

Fig. 11 - Experimental waveforms under high-speed command of 1200 rpm and load-torque of 1.0 N (a) MPCC; (b) ADM-MPCC

In addition to the current command, the speed command is also performed to verify the performance between the ADM-MPCC and the conventional MPCC. Under this test, two sets of experimental works are shown herein. Figure 10 shows a low-speed command of 200rpm, and Fig. 11 shows a high-speed command of 1200rpm, both of which are loaded with a disturbance of a load torque of 1.0 N. It can be observed that heavy current ripples are present in the classical MPCC, which indicates a poor performance in current prediction. Conversely, applying two voltage vectors in each control cycle helps to significantly improve the current prediction strategy by using the adaptive switching mechanism of the proposed ADM-MPCC. In particular, Fig. 10 shows the percentage improvement of 37.99%, 29.54%,and 38.36% for ACR, ACR, and THD*i*, respectively. The same result can be viewed relative to Fig. 11. The complete summary of the result is shown in Table 3, where a performance comparison of the two methods demonstrates impressive reductions in current ripple, current errors, and harmonic distortion in the proposed ADM-MPCC.

Table 3 - Performance comparison

ExperimentalCases (Figures)	Parameters	Conventional MPCC	Proposed ADM-MPCC	Percentage Improvement
Fig. 6 (4A, 10Hz)	ACR (A)	0.335	0.196	41.49%
	ACE (A)	0.268	0.186	30.60%
	THD*i*%	2.154	1.298	39.74%
Fig. 7 (4A, 30Hz)	ACR (A)	0.732	0.438	40.16%
	ACE (A)	0.561	0.402	28.34%
	THD*i*%	11.263	7.219	35.91%
Fig. 8 (Current Reversal, -4A to 4A)	ACR (A)	0.462	0.308	33.33%
	ACE (A)	0.336	0.234	30.35%
	THD*i*%	12.539	9.023	28.04%
Fig. 9 (Current Step, 1A to 4A)	ACR (A)	0.563	0.297	47.25%
	ACE (A)	0.412	0.283	31.31%
	THD*i*%	10.238	6.275	38.71%
Fig. 10 (200rpm, 1.0N)	ACR (A)	1.216	0.754	37.99%
	ACE (A)	1.124	0.792	29.54%
	THD*i*%	15.432	9.512	38.36%
Fig. 11 (1200rpm, 1.0N)	ACR (A)	1.598	0.901	43.62%
	ACE (A)	1.501	1.042	30.58%
	THD*i*%	16.123	12.397	23.11%

5. Conclusion

An adaptive duty modulation is successfully implemented to MPCC, known as the proposed ADM-MPCC, for SPMSM drives. Compared with the conventional technique, the proposed scheme integrates duty ratio optimization and adaptive soft-switching mechanism of the predictive controller *via* successive applications of two applied voltage vectors in each sampling period. Therefore, a better dynamic response can be observed in their current waveforms under current and speed commands. Results from experimental works and analysis showed that the proposed control scheme of ADM-MPCC can significantly improve the steady-state and transient responses based on the current trackingand current error performance compared to the conventional or traditional MPCC. Quantitatively, the overall results comparing ACR, ACE, and %THD*i* showed average percentage improvements of 40.64%, 30.12%, and 33.97%, respectively, compared to conventional methods.

Acknowledgment

The authors fully acknowledged the Department of Electrical Engineering Isabela State University for supporting this work.

References

[1] Wang, H., Lu, K., Wang, D., and Blaabjerg, F. (2020). Simple and effective online position error compensation method for sensorless SPMSM drives. IEEE Transactions on Industry Applications, vol. 56, no. 2, pp. 1475-1484.

[2] Agustin, C. A., Yu, J. -T., Lin, C. -K., Jai, J., and Lai, Y. -S. (2021). Triple-voltage-vector model-free predictive current control for four-switch three-phase inverter-fed SPMSM based on discrete-space-vector modulation.

IEEEAccess, vol. 9, pp. 60352-60363.
[3] Rodriguez, J., and Cortes, P. (2012). Predictive control of power converters and electrical drives, John Wiley & Sons.
[4] Li, Y., Qu, Y., Meng, X., Shi, H., and Jiao, S. (2017). Voltage vector selection strategy of the DTC for SPMSM based on predictive control. 20th International Conference on Electrical Machines and Systems (ICEMS), Sydney,NSW, pp. 1-4.
[5] Anh, H., Kien, C., Huan, T., and Khanh, P. (2018). Advanced speed control of PMSM motor using neural FOC method. 4th International Conference on Green Technology and Sustainable Development (GTSD), Ho Chi Minh,pp. 696-701.
[6] Sultan, N., Md Zain, B. A., Anuar, F. F.., Yahya, M., Abdul Latif, I.., Hat, M., & Al-alimi, S. (2019). Modeling andSpeed Control for Sensorless DC Motor BLDC Based on Real Time Experiment. International Journal of Integrated Engineering, 11(8), 55-64.
[7] Parchomiuk, M., Strzelecki, R., Zymmer, K., and Domino, A. (2017). Modular power converter with superconducting magnetic energy storage for electric power distribution system — analysis and simulation. 19th European Conference on Power Electronics and Applications (EPE'17 ECCE Europe), Warsaw, 2017, pp. P.1-P.6.
[8] Yan, L., Dou, M., and Hua, Z. (2019) Disturbance compensation-based model predictive flux control of SPMSM with optimal duty cyc. IEEE Journal of Emerging and Selected Topics in Power Electronics, vol. 7, no. 3, pp. 1872-1882.
[9] Wang, H., Lu, K., Wang, D., and Blaabjerg, F. (2020). Simple and effective online position error compensation method for sensorless SPMSM drives. IEEE Transactions on Industry Applications, vol. 56, no. 2, pp. 1475-1484.
[10] Widjonarko, Setiawan, A., Rudiyanto, B., Budi Utomo, S., & Setiyo, M. (2021). Characteristic of Fuzzy, ANN, and ANFIS for Brushless DC Motor Controller: An Evaluation by Dynamic Test. International Journal of Integrated Engineering, 13(6), 274-284.
[11] Rodriguez, J., Pontt, J., Silva, C. A., Correa, P., Lezana, P., Cortes, P., and Ammann, U. (2007). Predictive currentcontrol of a voltage source inverter. IEEE Transaction on Industrial Electronics, vol. 54, no. 1, pp. 495-503.
[12] Agustin, C. A., Yu J. -T., Cheng, Y. -S., Lin, C. -K., and Yi, Y. -W. (2021). A synchronized current difference updating technique for model-free predictive current control of PMSM drives. IEEE Access, vol. 9, pp. 63306-63318.
[13] Agustin, C. A, Yu, J.-T, Lin, C.-K., and Fu, X.-Y (2019). A modulated model predictive current controller for interior permanent-magnet synchronous motor. Energies, vol. 12, no. 15, pp. 2885.
[14] Parvathy, M. L., Eshwar K., Thippiripati, A (2021). A modified duty-modulated predictive current control for permanent magnet synchronous motor drive. IET ELectrica Power Applications, vol. 15, no. 1, pp. 25-38.
[15] Yu, X.-Y., and Li, Y.-Z (2022). Vector control of permanent magnet synchronous motor based on MRAS method.The International Journal of Multiphysics, vol. 16, no. 2, pp. 119-135.
[16] Lin, C.-K., Liu, T.-H., Yu, J.-T., Fu, L.-C., and Hsiao, C.-F. (2014). Model-free predictive current control for interior permanent-magnet synchronous motor drives based on current difference detection technique. IEEE Transactions on Industrial Electronics, vol. 61, no. 2, pp. 667-681.
[17] Cortes, P., Rodriguez, J., Silva, C., and Flores, A. (2012). Delay compensation in model predictive current control of a three-phase inverter. IEEE Transaction on Industrial Electronics, vol. 59, no. 2, pp. 1323-1325.